Interannual Variability in the Boreal Summer Intraseasonal Oscillation Modulates the Meridional Migration of Western North Pacific Tropical Cyclone Genesis

SHUFEN ZHANG,[a] HAIKUN ZHAO,[a] PHILIP J. KLOTZBACH,[b] XIANAN JIANG,[c,d] GUOSEN CHEN,[a] AND SHAOHUA CHEN[a]

[a] *Key Laboratory of Meteorological Disaster, Ministry of Education, Joint International Research Laboratory of Climate and Environment Change, Collaborative Innovation Center on Forecast and Evaluation of Meteorological Disaster, Pacific Typhoon Research Center, Earth System Modeling Center, Nanjing University of Information Science and Technology, Nanjing, China*
[b] *Department of Atmospheric Science, Colorado State University, Fort Collins, Colorado*
[c] *Joint Institute for Regional Earth System Science and Engineering, University of California, Los Angeles, Los Angeles, California*
[d] *Jet Propulsion Laboratory, California Institute of Technology, Pasadena, California*

(Manuscript received 31 May 2022, in final form 28 February 2023, accepted 14 March 2023)

ABSTRACT: Prior studies have emphasized the influence of the boreal summer intraseasonal oscillation (BSISO) on basin-scale and global-scale tropical cyclones (TCs). An improved understanding of the BSISO's impact on TCs at various climate time scales will likely lead to improved subseasonal-to-seasonal prediction. This study explores the impact of BSISO interannual variability on western North Pacific (WNP) TCs. We find that interannual meridional variability in the BSISO modulates the meridional migration of WNP TC genesis and is related to changes in BSISO phase structure. These structural changes are characterized by occurrence frequency changes for individual BSISO phases between the equatorial region over the eastern Indian Ocean (EIO)–Maritime Continent (MC) and the subtropical region over the South China Sea (SCS)–western Pacific. This interannual north–south change of the BSISO appears to be associated with changes in sea surface temperature over the MC region and WNP mid-to-low-tropospheric moisture advection, mainly via remote forcing of a Gill-type Rossby response to BSISO convection and a large meridional asymmetry of the low-level background moisture distribution. During years with increased BSISO residence time over the subtropical SCS–western Pacific, more TCs occur over the northern WNP due to TC-favorable BSISO-associated convection and circulation. In contrast, more TCs occur over the southern WNP in years with increased BSISO convection residence time over the equatorial EIO–MC. We find that the increase in frequency of BSISO phase occurrence over the subtropical SCS–western Pacific since the late 1990s has potentially contributed to a recent poleward shift of WNP TC genesis.

KEYWORDS: Madden–Julian oscillation; Tropical cyclones; Interannual variability

1. Introduction

The Madden–Julian oscillation (MJO; Madden and Julian 1971) has been recognized as a dominant mode of tropical intraseasonal variability with significant impacts on global weather and climate via both its direct tropical impacts and its extratropical teleconnections (Nakazawa 1988; Liebmann et al. 1994; Kim et al. 2008; Zhang 2013; Wang and Moon 2017; Wang et al. 2019; Chen and Wang 2021; Liu et al. 2022). Several studies have documented that the MJO has pronounced seasonality and regionality, with the boreal summer MJO also being referred to as the boreal summer intraseasonal oscillation (BSISO) (Yasunari 1979; Lau and Chan 1985; Wang and Rui 1990; Wang and Xie 1997; Zhang and Dong 2004; Kikuchi et al. 2012; Adames et al. 2016; Lee et al. 2013). Over the East Asian monsoon region, the BSISO propagates both eastward and northward (Yasunari 1979, 1981; Wang and Rui 1990; Hsu and Weng 2001; Hsu et al. 2004; Jiang et al. 2004; Kikuchi et al. 2012; Lee et al. 2013; Hsu et al. 2016; Chen and Wang 2021), which can cause significant impacts on weather events including heavy rainfall, floods, droughts, and tropical cyclone (TC) activity over highly populated portions of East Asia. As an important driver of intraseasonal TC activity and as a potential bridge for seamless temporal TC prediction (Wheeler and Weickmann 2001; Zhang 2013; Ren et al. 2018; Nakano et al. 2021; Zhao et al. 2022), skillful BSISO forecasts are of both socioeconomic value and scientific merit.

On subseasonal time scales, there is a general consensus that the BSISO strongly modulates western North Pacific (WNP) TCs, with more TCs forming during the convectively active phase (Nakazawa 1986; Liebmann et al. 1994; Kim et al. 2008; Camargo et al. 2009; Li and Zhou 2013; Zhao et al. 2015a,b, 2018; Zhao and Li 2019; Qin et al. 2023). Prior studies have suggested that the strong TC modulation by the BSISO is due to the BSISO's modulation of the large-scale atmospheric and oceanic environment as well as changes in prior tropical synoptic-scale disturbances by BSISO-associated Rossby wave energy accumulation (Sobel and Bretherton 1999; Sobel and Maloney 2000; Maloney and Dickinson 2003; Camargo et al. 2009; Huang et al. 2011; Zhao et al. 2015a,b, 2018, 2019a). Several studies have used the genesis potential index proposed by Emanuel and Nolan (2004) to assess the relative role of large-scale factors associated with the BSISO in modulating TCs and have found that the BSISO's primary

Corresponding author: Haikun Zhao, zhk2004y@gmail.com, haikunzhao@nuist.edu.cn

DOI: 10.1175/JCLI-D-22-0406.1

large-scale modulations that impact TCs are midlevel relative humidity and low-level vorticity (Camargo et al. 2009; Zhao et al. 2015a,b).

On the intraseasonal time scale, a new TC genesis potential index has been proposed by identifying the major factors associated with intraseasonal oscillations that affect global-scale and regional-scale TC genesis potential (Wang and Moon 2017; Moon et al. 2018). Tropical synoptic-scale disturbances that serve as TC precursors can amplify over the WNP basin due to lower-tropospheric Rossby wave accumulation caused by BSISO-associated large-scale convergence (Holland 1995; Sobel and Bretherton 1999; Sobel and Maloney 2000; Huang et al. 2011; Zhao et al. 2018, 2019a). Using empirical orthogonal function (EOF) analyses, Zhao et al. (2019a) investigated the association of boreal summer WNP TC genesis with various tropical waves. They found that the BSISO strongly enhanced ~70% of TCs through generation of a more favorable environment and modulation of the synoptic-scale wave train due to barotropic energy accumulation over the WNP monsoon region.

Changes in the large-scale environment and associated air–sea interactions in response to both natural variability and human-induced global warming cause modulations in the BSISO (Teng and Wang 2003; Kim et al. 2008; Kikuchi and Wang 2009; Yun et al. 2010; Tao et al. 2015; Yamaura and Kajikawa 2017; Bui and Maloney 2019; Lin 2019; Roxy et al. 2019; Dasgupta et al. 2021). These modulations then result in TC activity changes. For example, the tropical Pacific climate regime shift that occurred in the late 1990s caused interdecadal changes in the BSISO (Yamaura and Kajikawa 2017; Wu et al. 2021). Roxy et al. (2019) found that the recent expansion of the Indo-Pacific warm pool significantly distorted the MJO life cycle, with its residence time decreasing over the Indian Ocean by 3–4 days and increasing over the Indo-Pacific Maritime Continent by 5–6 days. Recently, there has been a growing body of literature examining BSISO changes in a warming climate. Under a high-emissions scenario, Zhou et al. (2020) found amplified BSISO impacts in the Pacific–North America region based upon a CMIP5 multimodel ensemble. Other studies have found that a warming climate may produce differing signals in BSISO precipitation intensity compared with BSISO wind intensity, thus leading to different impacts on weather and climate events (Wolding et al. 2017; Maloney et al. 2019).

The BSISO undergoes significant variability (Lin and Li 2008; Liu et al. 2016; Lin 2019; Chen and Wang 2021) on interannual time scales. Lin (2019) found that interannual variability of the BSISO is closely associated with the prior spring–winter ENSO-associated large-scale environment. Following El Niño, the subtropical anticyclonic anomaly over the WNP and negative moisture anomalies hinder BSISO northward propagation, causing the BSISO convection to linger in the Maritime Continent (MC) region. By contrast, cyclonic anomalies over the subtropical WNP and associated positive moisture anomalies following La Niña promote BSISO northward propagation. BSISO periodicity and propagation can be impacted through ENSO-induced background-mean-state changes, especially via mean moisture and vertical wind shear anomalies in the WNP (Liu et al. 2016). Prior studies also emphasized the role of large-scale moisture gradient and changes of warm pool sea surface temperature (SST) as well as their combined impacts on intraseasonal oscillations (Jiang et al. 2018; Kim 2017; Suematsu and Miura 2018; Roxy et al. 2019; Suematsu et al. 2022; Wang and Sobel 2022; Cai et al. 2022). The combined impact of ENSO and the BSISO on WNP TCs and the distinct impacts of different BSISO-associated propagation and intensity responses to ENSO have also been discussed (Lin and Li 2008; Liu et al. 2016; Lin 2019; Han et al. 2020; Sobel and Maloney 2000).

These prior studies document that the BSISO undergoes variability on multiple time scales that thus impacts both weather and climate. Prior studies have focused on the impact of the BSISO on boreal summer WNP TCs on intraseasonal time scales (Camargo et al. 2009; Li and Zhou 2013; Zhao et al. 2015a,b, 2018; Zhao and Li 2019), while the BSISO's impacts on WNP TCs on other time scales remains limited. This study examines how interannual variability of the BSISO influences summer WNP TC genesis.

The remainder of this study is arranged as follows. Section 2 describes the data used in this study as well as the methodology for identifying BSISO phases. Section 3 presents the main results of this study and examines interannual meridional BSISO variability and its impact on summer WNP TCs. Section 4 includes associated physical explanations for how the BSISO impacts WNP TCs. Section 5 discusses implications for the recent poleward shift in WNP TC genesis from interdecadal changes in interannual BSISO variability. A summary and discussion are given in section 6.

2. Data and methodology

a. TC data and reanalysis data

WNP TC data including 6-h-interval latitude, longitude, and maximum sustained wind are provided by the Joint Typhoon Warning Center (JTWC) (Chu 2002). All TCs with maximum 1-min sustained wind of 34 kt (1 kt $\approx$ 0.51 m s^{-1}) or greater are considered. We focus on WNP TC genesis frequency and TC genesis during extended summer, defined as May to October in this study, from 1980 to 2019. Daily outgoing longwave radiation (OLR) is obtained from the National Oceanic and Atmospheric Administration (NOAA). Daily wind at 850 hPa (U850) is obtained from the National Centers for Environmental Prediction–Department of Energy Reanalysis 2 (NCEP-DOE Reanalysis 2; Kanamitsu et al. 2002) with a horizontal resolution of 2.5° × 2.5° and 17 vertical pressure levels. These winds are used to identify BSISO phases and investigate the propagation of BSISO-associated convection and circulation. To further explore the interannual variability of the BSISO and its impact on TCs, we examine monthly SST data with a horizontal resolution of 2.0° × 2.0° from the NOAA Extended Reconstructed SST, version 5 (ERSSTv5; Huang et al. 2017). We include additional monthly atmospheric fields from the NCEP-DOE Reanalysis 2 project. The Niño-3.4 index, defined as average SST anomalies (SSTAs) within 5°S–5°N, 170°–120°W, is used to define ENSO events.

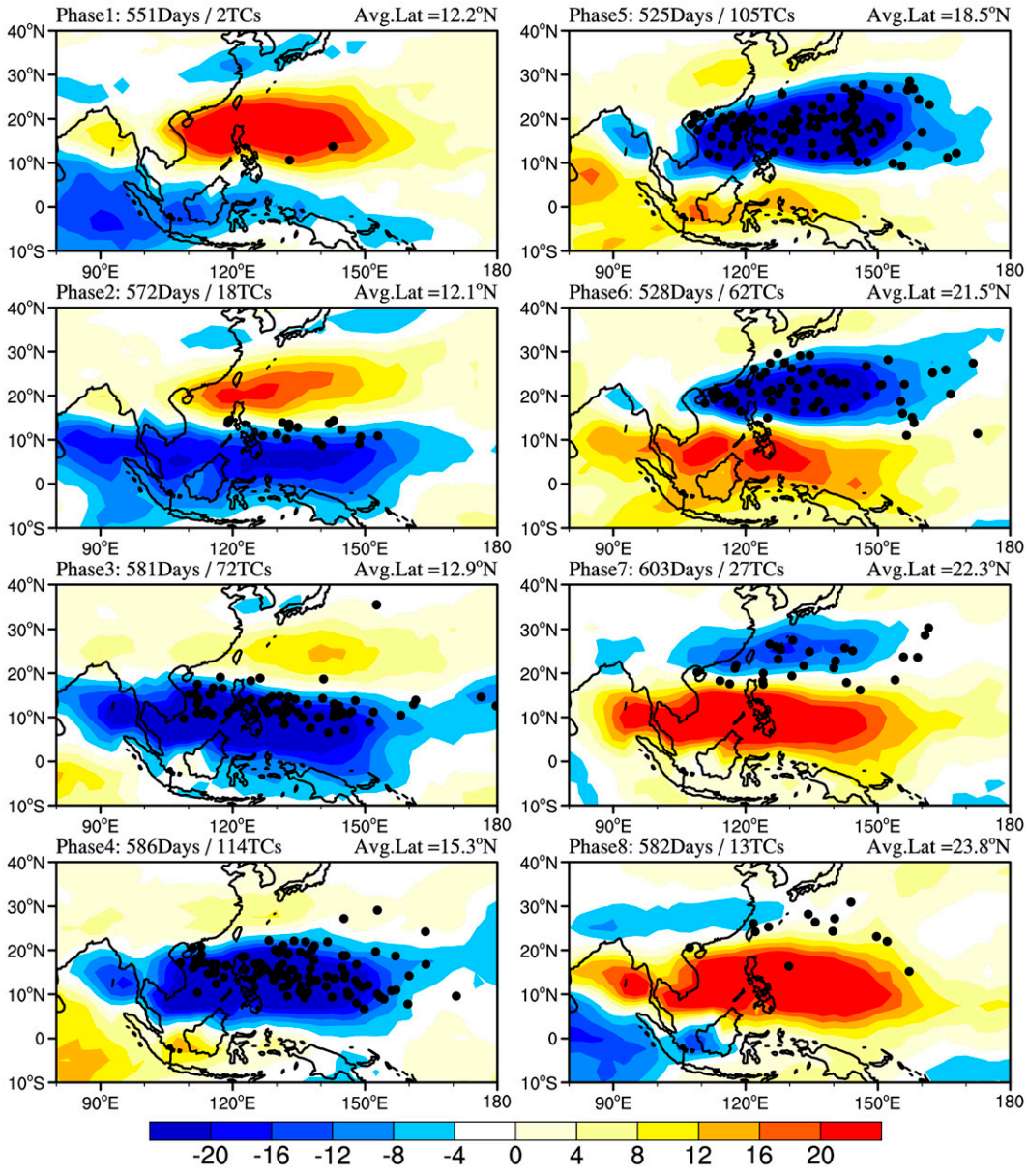

FIG. 1. Composite of OLR anomalies (shaded; W m^{-2}) for the eight BSISO phases, along with TC genesis locations over the WNP basin (dots). TC genesis frequency and phase occurrence days, as well as average TC genesis latitude, are shown for each BSISO phase.

b. *Identification of BSISO phases*

Following Wheeler and Hendon (2004), the BSISO indices are extracted using three steps: 1) the first three harmonics are removed to filter out seasonal variations from unfiltered daily OLR and U850 for each grid point over the region (10°S–40°N, 90°–150°E), 2) the prior 120-day average from each day is subtracted to remove the effects of most interannual variations including ENSO, and 3) the multivariate empirical orthogonal function (MV-EOF) modes are obtained from zonally averaged OLR and U850 from 90° to 150°E. Our BSISO indices are derived from the first two leading EOF modes (i.e., $EOF1_{BSISO}$ and $EOF2_{BSISO}$) and compare well to the BSISO indices obtained by Lee et al. (2013). These two BSISO indices describe a large fraction of total intraseasonal oscillation (ISO) variability in the East Asian monsoon–WNP region and have a good representation of the northward-propagating features of the BSISO (Wang and Xie 1997; Hsu and Weng 2001; Jiang et al. 2004; Lee et al. 2013; Liu et al. 2018). We divide the BSISO life cycle into eight phases and count days in each BSISO phase when they have an amplitude ($\sqrt{PC1^2_{BSISO} + PC2^2_{BSISO}}$, where PC1 and PC2 are the first and second principal components) greater than 1.0.

Additionally, we note that TCs occurring during these BSISO phases do not guarantee that all of these TCs were directly modulated by the BSISO (Jiang et al. 2012; Zhao et al. 2015a,b). In this study, TCs directly associated with the BSISO are further selected following Zhao et al. (2019a). A TC genesis case is attributed to the BSISO based upon two criteria:

1) The EOF-based reconstructed OLR anomalies are below zero in the 5° × 5° box with the center of the TC genesis location at the TC genesis time. The EOF-based reconstructed OLR anomaly for BSISO is computed as

$$\text{OLR} - \text{BSISO} = \text{PC1}_{\text{BSISO}} \times \text{EOF1}_{\text{OLR-BSISO}} + \text{PC2}_{\text{BSISO}} \times \text{EOF2}_{\text{OLR-BSISO}}, \quad (1)$$

where $\text{EOF1}_{\text{BSISO-OLR}}$ ($\text{EOF2}_{\text{BSISO-OLR}}$) is the regression pattern of OLR onto PC1 (PC2), respectively.

2) The wave amplitude of BSISO exceeds 1.0 at the TC genesis time.

Based on this identification, 416 TCs directly associated with the BSISO are selected, accounting for ~50% of the total number of WNP TCs in our study (835 TCs). In the following analysis, the TCs directly associated with the BSISO are used to compare with all TCs over the WNP basin, unless otherwise stated.

c. *Representation of interannual variability of BSISO phase frequency*

To better investigate the interannual variability of the BSISO, we use an approach similar to that described in prior studies (Lin et al. 2015; Lin 2019; Dasgupta et al. 2021). We count the number of days that each BSISO phase has an amplitude greater than one from May to October. The frequency of BSISO phase occurrence is therefore a function of BSISO phase and year from 1980 to 2019. These data are then used to perform an EOF analysis to identify the dominant phase structure of the interannual variability of the BSISO. This study focuses on the first EOF pattern and the corresponding PC1.

d. *Decomposition of the mean latitude of TC location metrics*

To measure the contribution of TC genesis frequency to average latitude, the latitude is decomposed using a method described in Feng et al. (2021). The mean latitude (LAT) of TC genesis for each group (e.g., positive and negative PC1) shown in expression (2) is determined by multiplying the sum of the latitude of TC genesis for each group (LAT_m) and the relative frequency P_m, where P_m is calculated as the ratio of TC genesis frequency in each group (N_m) to the total TC frequency in all groups (N_a):

$$\text{LAT} = \sum_m (\text{LAT}_m \times P_m), \quad P_m = \frac{N_m}{N_a}. \quad (2)$$

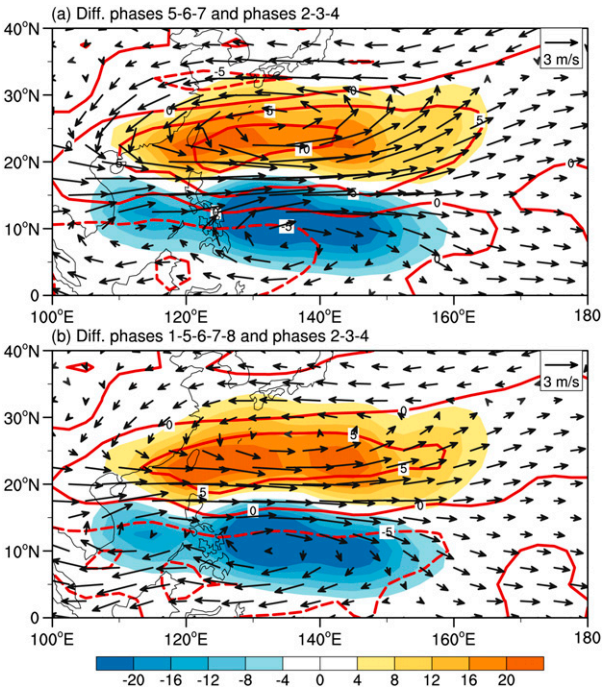

FIG. 2. Composite difference of the spatial distribution of TC genesis frequency (shaded) with 850-hPa winds (vectors; reference vector at top right of each panel) and midlevel relative humidity (contours; %) between (a) phases 5–7 and phases 2–4 and (b) phases 1 and 5–8 and phases 2–4.

Both LAT_m and P_m can be decomposed into a climatological mean latitude ($\overline{\text{LAT}_m}$, $\overline{P_m}$) and an anomaly (LAT'_m, P'_m) from the mean value. The latitude in each group can be expressed as

$$\begin{aligned}\text{LAT} &= \sum_m (\overline{\text{LAT}_m} + \text{LAT}'_m) \times (\overline{P_m} + P'_m) \\ &= \sum_m (\overline{\text{LAT}_m}\,\overline{P_m} + \overline{\text{LAT}_m} P'_m + \text{LAT}'_m \overline{P_m} + \text{LAT}'_m P'_m) \\ &= \overline{\delta} + \delta_P + \delta_{\text{LAT}} + \delta_{\text{LATP}}, \end{aligned} \quad (3)$$

where δ_{LAT} and δ_P denote the contribution of the relative frequency (P') and latitudinal deviation (LAT′) to the mean latitude for each group, respectively, and δ_{LATP} denotes the interannual covariance between LAT′ and P'. Similarly, the groups represented by years with positive and negative PC1 are used to explore the contributions of relative frequency to the mean latitude between years with increased frequency of individual BSISO phase occurrences. These results have implications for the poleward shift of TC genesis over the WNP basin during recent decades. A similar decomposition method has been used to quantify the contribution of interbasin frequency changes to the global poleward migration of TC tracks (Moon et al. 2015).

e. *Statistical significance tests*

The statistical significance of correlations and differences of means is performed using the two-tailed Student's

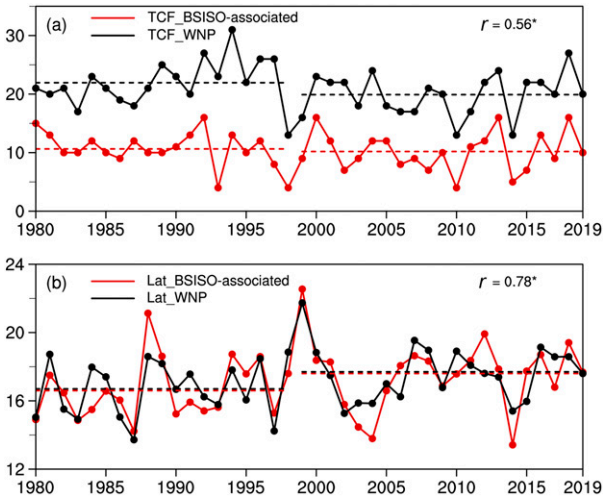

FIG. 3. (a) Time series of TC genesis frequency over the WNP during May–October for the period 1980–2019 (black) and TC genesis frequency directly associated with the BSISO (red). (b) As in (a), but for TC genesis latitude. Correlations between the two time series are also calculated. The dashed lines show the mean values for (a) TC genesis frequency and (b) TC genesis latitude for the 1980–98 and 1998–2019 periods, respectively. An asterisk indicates that the correlation is significant at a 95% confidence level.

t test. We test for statistical significance at the 0.05 level in this study.

3. Interannual variability of BSISO modulates WNP TC meridional migration

a. Spatial association between the BSISO and TC variability

Figure 1 shows the evolution of BSISO phases along with summer TC genesis over the WNP basin during the period 1980–2019. We find good consistency between BSISO-associated convection and TC genesis events directly associated with the BSISO. In response to eastward and northward propagation of the BSISO, the favored locations for WNP TC genesis also change. During BSISO phases 2–4, where associated convection is mainly located over the tropical eastern Indian Ocean (EIO)–MC, more TCs form over the southern WNP region, with an average TC genesis latitude of ~14.2°N. By contrast, more TCs tend to occur over the northern WNP region during phases 5–7, with an average TC genesis latitude of ~20.0°N. These BSISO phases are associated with enhanced convection over the subtropical South China Sea (SCS) and the western Pacific. The difference in average TC genesis latitude of 5.8° between phases 2–4 and phases 5–7 is significant. The spatial differences in TC genesis also exhibit a distinct north–south meridional dipole pattern (Fig. 2a), corresponding to changes in both low-level winds and midlevel relative humidity. This strong climatological modulation of WNP TCs by the BSISO was also found in prior studies and can be explained by changes in large-scale environmental factors

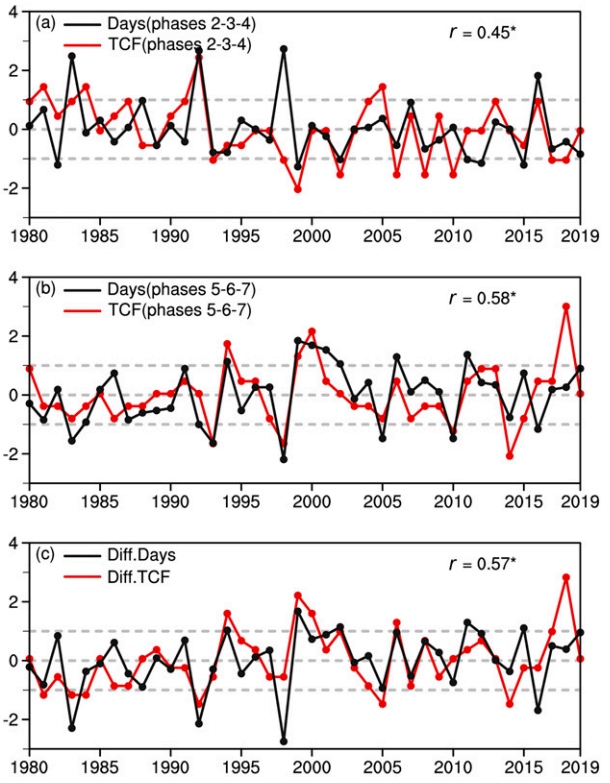

FIG. 4. Standardized time series of TC genesis frequency and the frequency of occurrence (a) for phases 2–4, (b) for phases 5–7, and (c) for the difference between phases 5–7 and phases 2–4. Correlation coefficients between the frequency of BSISO phase occurrence and TC genesis frequency are also shown. An asterisk indicates that the correlation is significant at a 95% confidence level.

associated with the BSISO (Camargo et al. 2009; Li and Zhou 2013; Zhao et al. 2015a,b, 2018; Zhao and Li 2019).

b. Interannual association between the BSISO and TC variability

On the interannual time scale, there is a significant correlation between BSISO-associated TC frequency and the total number of summer WNP TCs (Fig. 3a) ($r = 0.56$). Similar results are found for TC genesis latitude (Fig. 3b). The average TC genesis latitude during all eight BSISO phases significantly correlates with the average TC genesis latitude for all summer TCs over the whole WNP basin ($r = 0.78$). This relationship implies that TC genesis latitude during all eight BSISO phases captures ~50% of the variance of total WNP summer TC genesis latitude from 1980 to 2019. We next compute TC genesis frequency and the frequency of BSISO phases 5–7 occurrence, indicating that enhanced BSISO-associated convection spends more time in the subtropical SCS and western Pacific. We find a significant correlation ($r = 0.56$) between TC genesis frequency and BSISO phase 5–7 occurrence (Fig. 4b). A similar result is found for phases 2–4, with a significant correlation between TC genesis frequency and the frequency of BSISO phase occurrence ($r = 0.45$) (Fig. 4a). These results suggest

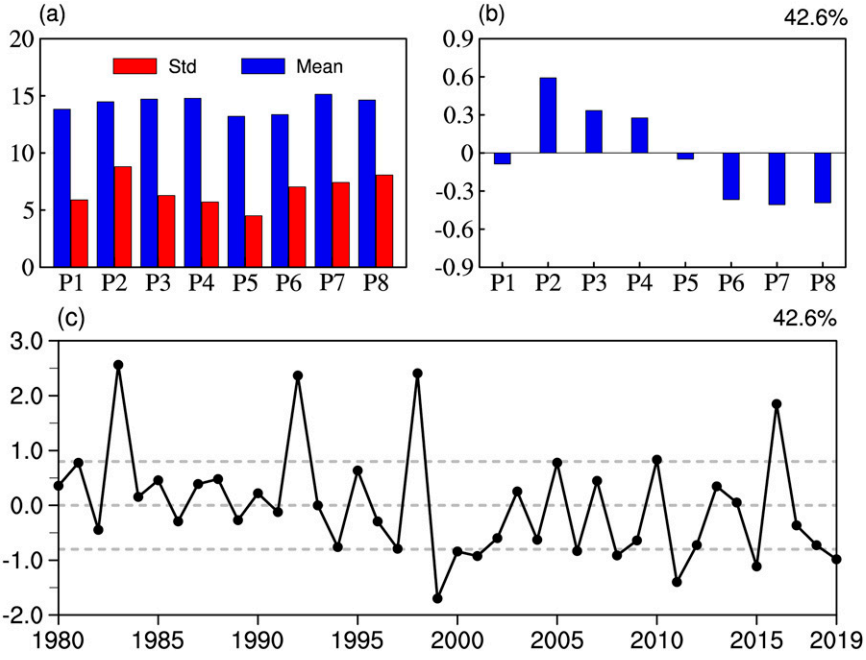

FIG. 5. (a) Average (blue) and interannual standard deviation (red) of the frequency of occurrence for BSISO phases from May to October. (b) The first EOF mode (EOF1) of the frequency of occurrence for BSISO phases and (c) the corresponding PC1. The percentage noted in the top-right corner of (b) and (c) is the variance explained.

that the meridional displacements of TC genesis associated with interannual changes in BSISO phase occurrence frequency play an important role in modulating the interannual variability of summer WNP TCs. Given that the total TC genesis frequency for all BSISO phases during the period 1980–2019 accounts for ~50% of summer WNP TC frequency, improved understanding of interannual changes in the BSISO and how they impact both TC genesis frequency and TC meridional migration may be useful for interannual prediction of WNP TCs.

c. *EOF analysis of the BSISO–WNP TC relationship*

To further support the importance of interannual variability in the BSISO in modulating TCs, we use EOF analyses to identify the dominant phase structure of the interannual variability of the BSISO (i.e., PC1) as shown in section 2c and investigate the impacts of interannual variability of the BSISO on summer WNP TCs. As shown in Fig. 5b, the first EOF mode (EOF1) of BSISO phase occurrence frequency shows a relatively large value in BSISO phases 2–4 and phases 6–8. We find similar behavior when investigating the mean and interannual standard deviation of the frequency of BSISO phase occurrence with relatively high-frequency values of phases 2–3 and phases 7–8 (Fig. 5a). These phases correspond to BSISO activity over the tropical EIO–MC and subtropical SCS–western Pacific, respectively. The first EOF mode explains ~42% of the variance and can be separated from other EOF modes based upon the rules proposed by North et al. (1982).

As shown by the dominant phase structure of interannual variability of the BSISO (Fig. 5b), we find an obvious shift of the frequency of BSISO phase occurrence with negative anomalies for phases 1 and 5–8 and positive anomalies for phases 2–4. As seen in Figs. 6a and 6b, more TCs occur over the SCS-subtropical region during negative PC1 years, and more TCs occur over the tropical WNP during positive PC1 years. This result indicates an apparent northward shift of TC genesis in negative PC1 years compared with during positive PC1 years (from 16.5° to 17.8°N). This poleward shift in TC genesis during negative PC1 years compared with during positive PC1 years is further confirmed by the difference in TC genesis distribution for phases 2–4, for phases 1 and 5–8, and for all eight phases (Fig. 6c). A clearer south–north dipole pattern of TC genesis distribution can be seen (Fig. 6c, shading) for all eight BSISO phases when examining strong negative and positive PC1 years [defined as PC1 magnitude >0.8 standard deviations (STD) based upon the time series of PC1 as shown in Fig. 5c]. More TCs tend to form poleward for BSISO phases 1 and 5–8 during strong negative PC1 years (Fig. 6c, blue contours), while more TCs tend to form equatorward for BSISO phases 2–4 during strong positive PC1 years (Fig. 6c, red contours).

d. *Budget analysis of the intraseasonal genesis potential index*

As suggested above, marked changes in TC genesis events associated with the BSISO and its interannual variability are tied to BSISO-induced changes in the large-scale environment.

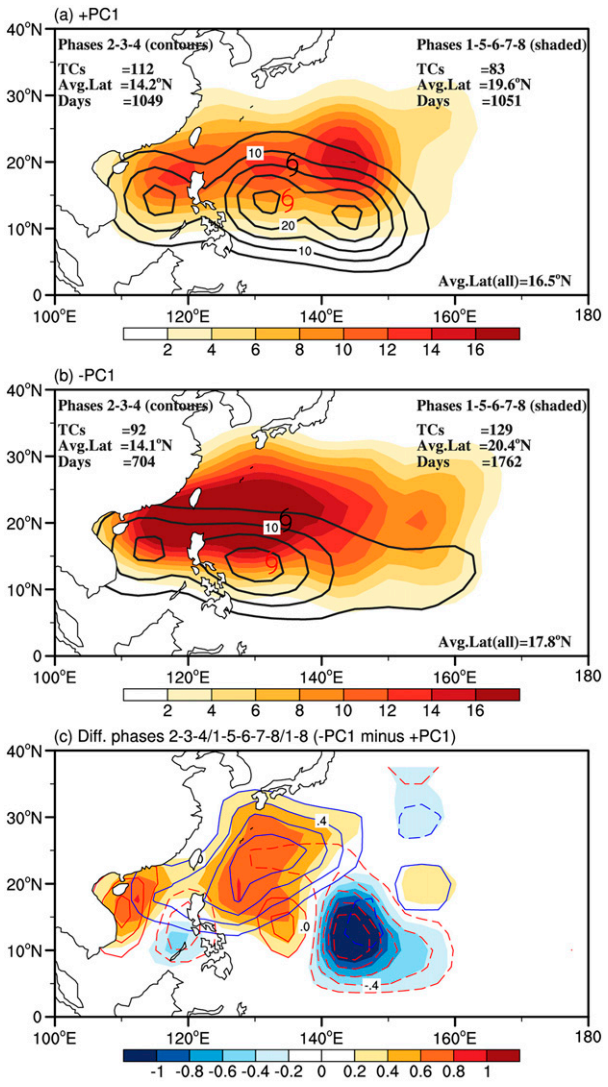

FIG. 6. Spatial distribution of TC genesis frequency for phases 2–4 (contours) and phases 1 and 5–8 (shaded) for years with (a) PC1 greater than 0 and (b) PC1 less than 0. The corresponding TC genesis frequency, the average TC genesis latitude, and the frequency of occurrence for phases 2–4 (phases 1 and 5–8) are shown in the top left (top right). The bottom-right value is the average latitude for all eight phases. (c) Difference of TC genesis distribution for BSISO phases 2–4 (red contours), phases 1 and 5–8 (blue contours), and all eight BSISO phases (shaded) between strong negative PC1 and positive PC1 years.

To further understand these changes, the intraseasonal genesis potential index (ISGPI) proposed by Wang and Moon (2017) and Moon et al. (2018) is used to explore the role of large-scale factors associated with the BSISO in modulating TC genesis. The ISGPI focuses on the contributions of three intraseasonal environmental variables: zonal wind shear (V_{zs}), 500-hPa vertical velocity (ω_{500}), and 850-hPa relative vorticity weighted by the Coriolis parameter: $f\zeta_{r850}$ to WNP TC genesis. The ISGPI is calculated using the following equation:

$$\text{ISGPI} = (-0.55) \times \omega_{500} + (0.22) \times f\zeta_{r850} + (-0.20) \times V_{zs}. \quad (4)$$

As shown in Fig. 7, the ISGPI successfully reproduces the spatial distribution of TC genesis in response to BSISO phase changes as well as interannual variability. The dipole pattern of TC genesis differences between phases 1 and 5–8 and phases 2–4 for the whole period of 1980–2019, for positive PC1 years and for negative PC1 years, respectively, is also explained by the ISGPI (Figs. 7a–c). A budget analysis of the ISGPI shows that TC genesis differences between phases 1 and 5–8 and phases 2–4 are due to the combined changes of the three factors included in the ISGPI, with different roles of large-scale factors for different regions.

From 1980 to 2019, 500-hPa vertical velocity and 850-hPa relative vorticity weighted by the Coriolis parameter are the two most important factors for the region from 20° to 30°N, with vertical wind shear playing a minor role. In contrast, all three factors are important for the 5° to 20°N region, with a positive contribution to the total ISGPI from 500-hPa vertical velocity and weighted 850-hPa relative vorticity and a negative contribution to the total ISGPI from vertical wind shear.

During positive PC1 years, 500-hPa vertical velocity is the most important factor in both regions, with the other two factors playing a limited role. However, during negative PC1 years, the vertical wind shear and 500-hPa vertical velocity appear to be the key factors, but the effect of vertical shear is opposite in the two regions. In comparison with the robust contribution from 500-hPa vertical velocity to ISGPI, the contribution from vertical shear is not systematic and is occasionally of the opposite sign to the total ISGPI. The 850-hPa relative vorticity is the same sign as the 500-hPa vertical velocity (and ISGPI) but with a smaller magnitude. Moon et al. (2018) argued that vertical velocity, relative vorticity, and humidity are highly correlated with each other. It is furthermore found that the total ISGPI anomalies in the 20°–30°N belt are weaker during negative PC1 years than during positive PC1 years, while there are no significant changes in the 5°–20°N belt. In positive PC1 years, with a seasonal mean anomalous anticyclonic circulation, tropical WNP ISGPI decreases owing to the reduction in upward motion in phases 1 and 5–8 relative to phases 2–4 (Figs. 7b,e). The same is true in negative PC1 years, with a seasonal mean anomalous cyclonic circulation, but with an increase in subtropical WNP ISGPI due to enhanced upward motion in phases 1 and 5–8 relative to phases 2–4 (Figs. 7c,f). The latter is collocated with increased midtropospheric humidity due to increased BSISO-associated moisture transport in negative PC1 relative to positive PC1 in the 20°–30°N belt, as a response to a BSISO-associated convective activity difference. The stronger reduction of upward motion in the tropical WNP in positive PC1 years relative to negative PC1 years may reflect more time in BSISO phases 2–4 (Figs. 1 and 7a,b) than in phases 1 and 5–8. In summary, these analyses suggest that changes in the TC environment associated with the BSISO and its interannual variability play an important role in modulating WNP TC genesis.

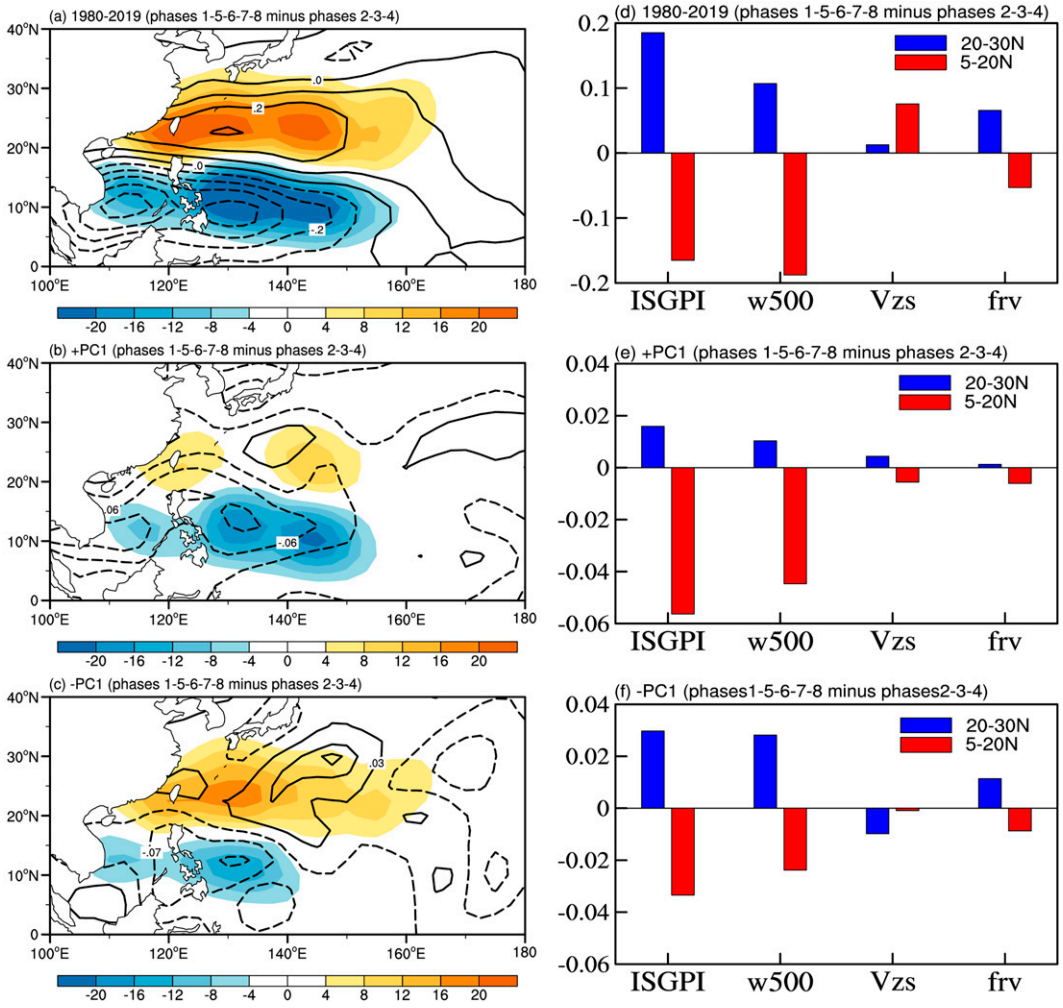

FIG. 7. Difference in the spatial distribution of TC genesis frequency (shaded) and ISGPI (contours) between phases 1 and 5–8 and phases 2–4 during (a) the period 1980–2019, (b) positive PC1 years, and (c) negative PC1 years. Contributions of the three terms to the total observed ISGPI anomalies from 5° to 20°N (red) and from 20° to 30°N (blue) between phases 1 and 5–8 and phases 2–4 during (d) the period 1980–2019, (e) positive PC1 years, and (f) negative PC1 years.

e. *Role of BSISO interannual variability in WNP TC modulation*

Given strong interannual variability of the BSISO, TC genesis frequency and TC genesis latitude undergo corresponding interannual changes. PC1 strongly correlates with the difference of the BSISO phase occurrence frequency between phases 1 and 5–8 and phases 2–4 ($r = -0.98$). This high correlation between PC1 and the corresponding BSISO phase occurrence frequency further indicates that the BSISO's impact on TCs is mainly via its residence time over different regions. Correspondingly, PC1 also strongly correlates with TC frequency differences between phases 1 and 5–8 and phases 2–4 ($r = -0.52$) (Fig. 8c). Similarly, the difference of phase occurrence frequency between phases 1 and 5–8 and phases 2–4 significantly correlates with TC genesis frequency differences ($r = 0.54$). The average TC genesis latitude for all boreal summer TCs during positive PC1 years is 16.5°N, while the average TC genesis latitude is 17.8°N during negative PC1 years (Figs. 6a,b).

To further emphasize the influence of interannual variability in the BSISO on WNP TCs, we select five strong positive PC1 years (i.e., 1983, 1992, 1998, 2010, and 2016) with increased frequency of phases 2–4 and nine strong negative PC1 years (i.e., 1997, 1999, 2000, 2001, 2006, 2008, 2011, 2015, and 2019) with increased frequency of phases 1 and 5–8 for performing composite analysis. Figure 9 shows distinct BSISO-associated convection propagation, with more obvious northward propagation during strong negative PC1 years (average TC genesis latitude of 18.3°N) compared with during strong positive PC1 years (average TC genesis latitude of 16.6°N). Correspondingly, more TCs tend to form poleward during strong negative PC1 years relative to during strong positive PC1 years, as shown in Fig. 6c. These meridional changes in TC genesis

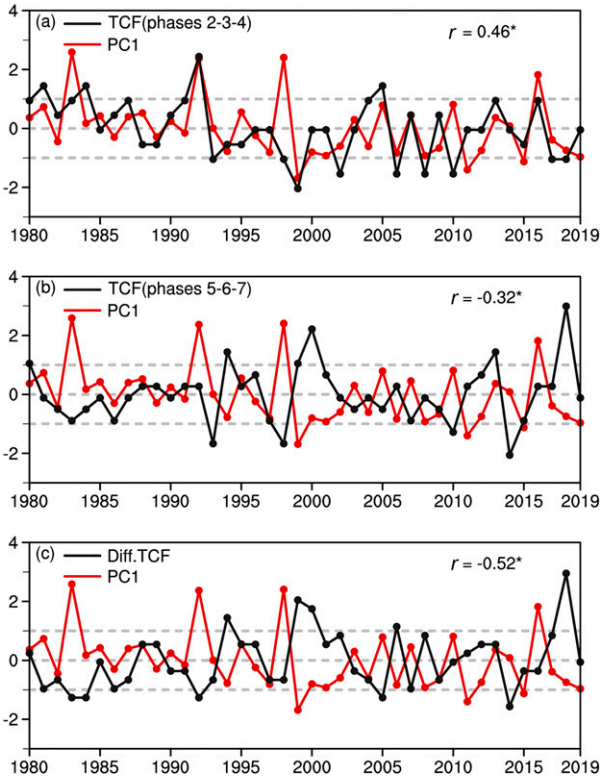

FIG. 8. Standardized time series of PC1 and TC genesis frequency for (a) phases 2–4 and (b) phases 1 and 5–8 and (c) the difference between phases 1 and 5–8 and phases 2–4. An asterisk indicates that the correlation is significant at a 95% confidence level.

between strong positive and strong negative PC1 years appear to be consistent with changes in the large-scale environment. There are increases in midlevel moisture and cyclonic anomalies over the WNP during strong negative PC1 years, when BSISO convection is favored over the subtropical SCS–western Pacific (Fig. 10c), favoring more TCs over the northern WNP. In contrast, in positive PC1 years, the TC-favorable environment, including increased midlevel moisture and westerly low-level wind anomalies, favors TCs over the southern WNP basin. In positive PC1 years, BSISO convection is preferentially located over the tropical EIO–MC.

4. Possible explanation for the BSISO–TC interannual relationship

The interannual variability of the BSISO impacts WNP TC meridional migration, mainly through modulation of the BSISO residence duration. During strong negative PC1 years, the BSISO propagates more northward at a stronger intensity with increased residence time over the WNP. This increased residence time is especially pronounced in the SCS and WNP, leading to an increased frequency of phases 1 and 5–8 occurrence and more TCs over the northern WNP (Figs. 6 and 9b). By contrast, during strong positive PC1 years, the center of BSISO convection tends to stay over the equatorial EIO–MC region with increased phases 2–4 occurrence frequency. This increase in frequency of phases 2–4 increases residence time at low latitudes, leading to increased TC genesis over the southern WNP (Figs. 6 and 9a). These are further confirmed by a significant correlation of −0.32 (0.46) between PC1 and TC genesis frequency for phases 1 and 5–8 (phases 2–4), respectively (Figs. 8a,b).

The interannual north–south displacement of BSISO convection is possibly associated with changes in Indo-Pacific warm pool SST (Fig. 10a). Prior studies have suggested the importance of SST in air–sea convective coupling, thus affecting ISO intensity and propagation (Pohl and Matthews 2007; Suematsu and Miura 2018; Suematsu et al. 2022; Roxy et al. 2019). As suggested in Roxy et al. (2019), that focused on the boreal winter, the area expansion of the Indo-Pacific warm pool in boreal summer could potentially slow down propagation of BSISO-associated convection and thereby adjust the BSISO life cycle. Warmer SSTAs over the tropical EIO–MC occur during strong positive PC1 years (Fig. 10a).

Additionally, the interannual variability of BSISO activity can be partly explained by changes in lower-tropospheric moisture advection on intraseasonal time scales (i.e., advection of mean moisture by BSISO-associated flow anomalies) (Jiang et al. 2004, 2018; Adames et al. 2016). As shown in Fig. 10b, there is strong positive horizontal moisture advection over the SCS–WNP region (15°–25°N, 100°–130°E) in the lower troposphere (from 900 to 600 hPa). This increased moisture advection is a result of enhanced southwesterly winds, thus favoring northward propagation of BSISO convection propagation and increasing residence time over the subtropical SCS–WNP during strong negative PC1 years.

As suggested in previous studies, seasonal mean moisture is significantly associated with ISO propagation (Sobel and Maloney 2013; Liu et al. 2016; Jiang 2017). As shown in Fig. 10c, collocated with the low-level cyclonic anomalies are positive specific humidity anomalies, implying that the eastward shift of the western Pacific subtropical high is accompanied by low-level convergence. Consequently, increased seasonally averaged specific humidity between 10° and 20°N (Fig. 10c) increases the meridional gradient of the background basic state moisture distribution, also favoring BSISO northward propagation. By contrast, in strong positive PC1 years, anticyclonic anomalies accompanied by negative moisture anomalies occur in the western WNP around 20°N, inhibiting northward convective propagation, thus increasing residence time of the BSISO in the equatorial EIO–MC.

Note that PC1 is found to be closely linked to prior spring–winter ENSO conditions, as shown in Fig. 11a, similar to the results of Lin (2019), who found that ENSO strongly impacted the BSISO in East Asia and the WNP. There is also a strong correlation between the previous winter ENSO and the difference in BSISO phase occurrence frequency and TC genesis frequency between phases 1 and 5–8 and phases 2–4 (Figs. 11b,c). This indicates that prior winter ENSO conditions can be a potential predictor in forecasting interannual variability of the BSISO and thus interannual variability in the WNP TC genesis distribution. ENSO can also affect the BSISO via changes in the background basic state circulation (Lin 2019; Lin and Li 2008; Liu et al. 2016). When the prior winter is characterized by El Niño, subsequent summer

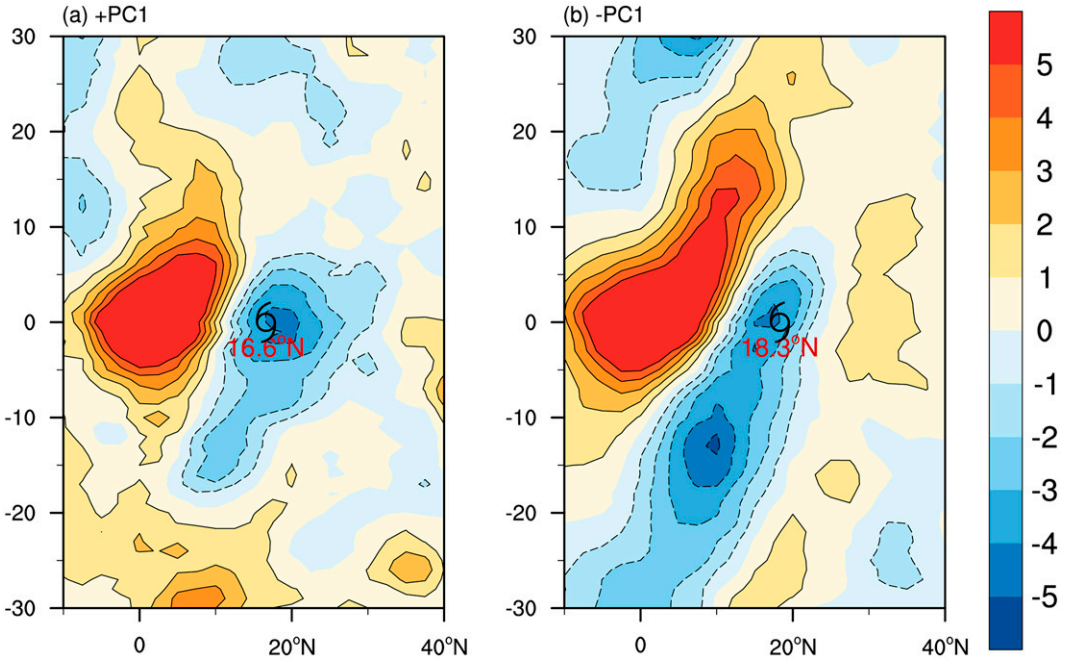

FIG. 9. (a) Lagged regressions of zonally averaged OLR anomaly from 90° to 150°E during the period May–October with PC1 > 0.8 STD. The reference time series is zonally averaged OLR anomaly on day 0 at the equator. (b) As in (a), but with PC1 < −0.8 STD. The averaged TC genesis location for strong positive PC1 years (16.6°N) and negative PC1 years (18.3°N) is marked with a black cyclone symbol.

BSISO activity typically becomes stronger, with increased residence time over the tropical EIO–MC, similar to the results of Pohl and Matthews (2007). In contrast, during years with prior winter La Niña, the summer BSISO tends to propagate northward, with associated BSISO convection prevailing over the subtropical SCS–WNP. The interannual modulation of the BSISO via prior El Niño (La Niña) may be associated with the evolution of an anomalous anticyclonic (cyclonic) circulation over the Philippines Sea through the Pacific–East Asian teleconnection (Wang et al. 2000), which then inhibits (favors) northward propagation of BSISO convection (Figs. 11d–f). These results are also supported by prior studies on the importance of prior ENSO on the predictability of the boreal summer monsoon and TC activity in East Asia via air–sea coupling processes (Takaya et al. 2021; Xie et al. 2009, 2016).

5. Implications for the recent poleward shift in TC genesis

Whether global warming has resulted in a poleward shift of global TCs is a topic of contention (Kossin et al. 2016; Song and Klotzbach 2018). However, studies have found that WNP TCs have undergone a significant poleward shift in recent decades (Liu and Chan 2013; Hu et al. 2018; Zhao et al. 2019b; Feng et al. 2021). Together with a poleward shift of TC genesis in negative PC1 years, as noted above, and more negative PC1 years since the late 1990s, as shown in Fig. 5c, we speculate that changes in TCs associated with the BSISO may have played an important role in the poleward shift of TC genesis latitude since the late 1990s. We first compared the average genesis latitude for TCs directly associated with the BSISO for two subperiods: 1980–98 and 1999–2020. We find a significant poleward shift of average genesis latitude for TCs directly associated with the BSISO from 16.6°N before 1998 to 17.7°N since 1998, which we find could be largely responsible for the significant poleward shift of summer WNP TC genesis from 16.7° to 17.7°N since 1998 (Fig. 3b).

We further examine shifts in meridional TC frequency associated with the BSISO for different groups of PC1 years, following the approach of Moon et al. (2015) and Feng et al. (2021) (see section 2d for more details on the decomposition method). As shown in Table 1, δ_{LAT} has a positive contribution to TC genesis latitude in both negative PC1 years and positive PC1 years, indicating that the influence of the background environmental moisture is favorable for the northward shift of TC genesis. The difference is that the frequency change term (δ_P) makes a positive contribution to TC genesis latitude during negative PC1 years, with a negative contribution during positive PC1 years. Given the small covariance amplitude δ_{LATP} of 0.1 for both negative and positive PC1 years, we find weak covariability between changes in relative TC frequency (P') and genesis latitude (LAT′). This weak relationship seems to be insufficient to account for a direct link between increases in TC frequency and the northward shift of TC genesis latitude during negative PC1 years.

As shown in section 3, more TCs tend to form poleward in strong negative PC1 years. There is a significant poleward

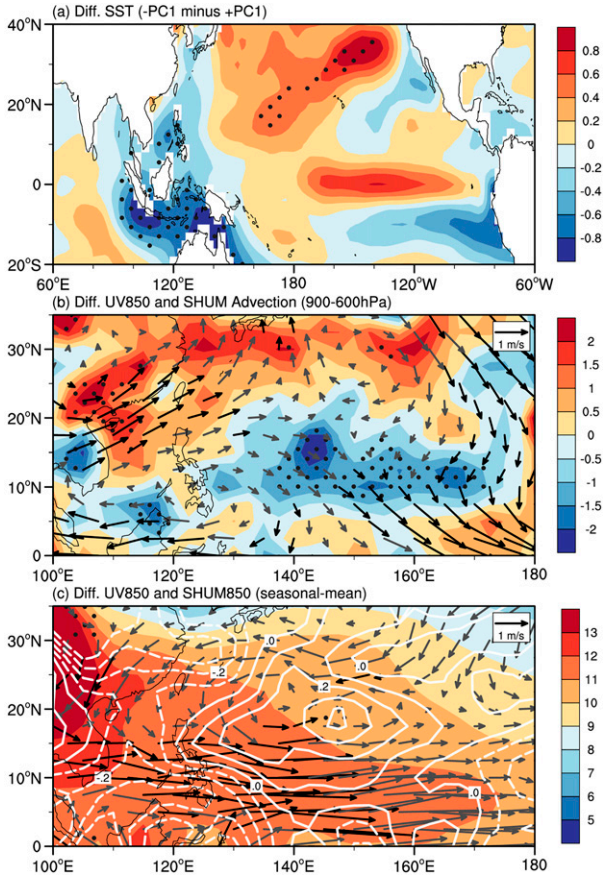

FIG. 10. (a) Composite SST difference between strong positive (>0.8 STD) and strong negative (<−0.8 STD) PC1 years. (b) As in (a), but for 850-hPa BSISO-associated winds (vectors; reference vector at top right) and mean lower-tropospheric (900–600 hPa) specific humidity advection (shaded; 10^2 s^{-1}). (c) As in (b), but for seasonal mean 850-hPa winds (vectors; reference vector at top right), 850-hPa specific humidity (contours; g kg^{-1}), and climatological-mean 850-hPa specific humidity (shaded; g kg^{-1}). Black vectors and black dots indicate significant correlations at a 95% confidence level.

shift of TC genesis during strong negative PC1 years (average TC genesis latitude of 18.3°N) compared with during strong positive PC1 years (average TC genesis latitude of 16.6°N). The difference of 1.7° between strong negative and strong positive PC1 years is considerably larger than the difference of 1.3° between all negative and positive PC1 years, highlighting the importance of PC1 strength in meridional shifts in TC genesis. We therefore reclassified our results into three groups to emphasize the role of changes in strong PC1 years in the poleward shift of TC genesis latitude (Table 2). As shown in Table 2, the magnitude of δ_{LAT} is the largest in strong negative PC1 years (0.42 compared with 0.10), when all background fields contribute positively to the latitudinal term. The covariance of δ_{LATP} is greater than 0 and has a large amplitude (0.30 compared with −0.03 and −0.02), indicating that the change in relative TC frequency and the genesis latitude are dependent on each other and change in the same direction. Based on these analyses, the poleward shift of annually averaged TC genesis latitude over the WNP since 1998 is substantially contributed to by an apparent increase in strong negative PC1 years, as shown in Fig. 5c. However, we also found a similar TC genesis distribution that is not associated with BSISO between strong negative PC1 and positive PC1 years. This result indicates that TCs not associated with the BSISO also substantially contribute to the poleward shift in WNP TCs. Additionally, the interannual correlation between total TC genesis frequency (~835 TCs) and TCs not associated with the BSISO (~419 TCs) is 0.62. In this sense, the BSISO-associated variation does not solely account for the interannual variability of the TC genesis latitude for all TCs in the WNP. Other potential factors deserve future study.

6. Summary

Prior studies have emphasized interannual modulations of TCs by the BSISO for specific basins as well as the globe (Liebmann et al. 1994; Maloney and Hartmann 2000a,b; Bessafi and Wheeler 2006; Aiyyer and Molinari 2008; Kim et al. 2008). This study explores the effects of interannual meridional variability of BSISO activity and its impacts on the meridional migration of WNP TCs. Strong negative (positive) PC1 years with increased residence time of phases 1 and 5–8 (phases 2–4) activity favor summer WNP TC genesis forming more northward (southward). Interannual meridional variability of BSISO activity appears to be associated with SST changes over the Indo-Pacific warm pool, especially over the MC region, along with associated changes in lower-tropospheric moisture advection tied to anomalous circulation patterns. Warming SSTAs located near the equatorial EIO–MC region during strong positive PC1 years cause slower BSISO propagation, with increased residence time over the southern WNP region. Increased moisture advection over the subtropical SCS–WNP region from enhanced southwesterly winds favor northward propagation of the BSISO, with increased residence time over the northern WNP region. The interannual change in BSISO is found to be associated with the prior winter ENSO state via ENSO-induced changes in the large-scale environment. Given the relationship with ENSO and ENSO's predictability, there is a potential for interannual prediction of the BSISO, and thus TC genesis distribution, over the WNP basin. To examine the simultaneous impact of ENSO from the relationship between the BSISO and TC genesis latitude, we computed the simultaneous relationship between May–October PC1 and the May–October Niño-3.4 index and found that their correlation from 1980 to 2019 was insignificant ($r = -0.16$). Similarly, when the simultaneous impact of boreal summer ENSO was removed from PC1, the difference in TC genesis frequency between BSISO phases 2–4 and phases 1 and 5–8 remained significantly associated with PC1 ($r = 0.61$). Similarly, we found that the simultaneous relationship between PC1 and difference in TC genesis frequency between BSISO phases 2–4 and phases 1 and 5–8 remains significant ($r = -0.56$) when excluding the strong simultaneous ENSO years based on a threshold of 0.8 standard of Niño-3.4 index. In this sense, simultaneous ENSO during boreal summer appears to play a limited role in modulating

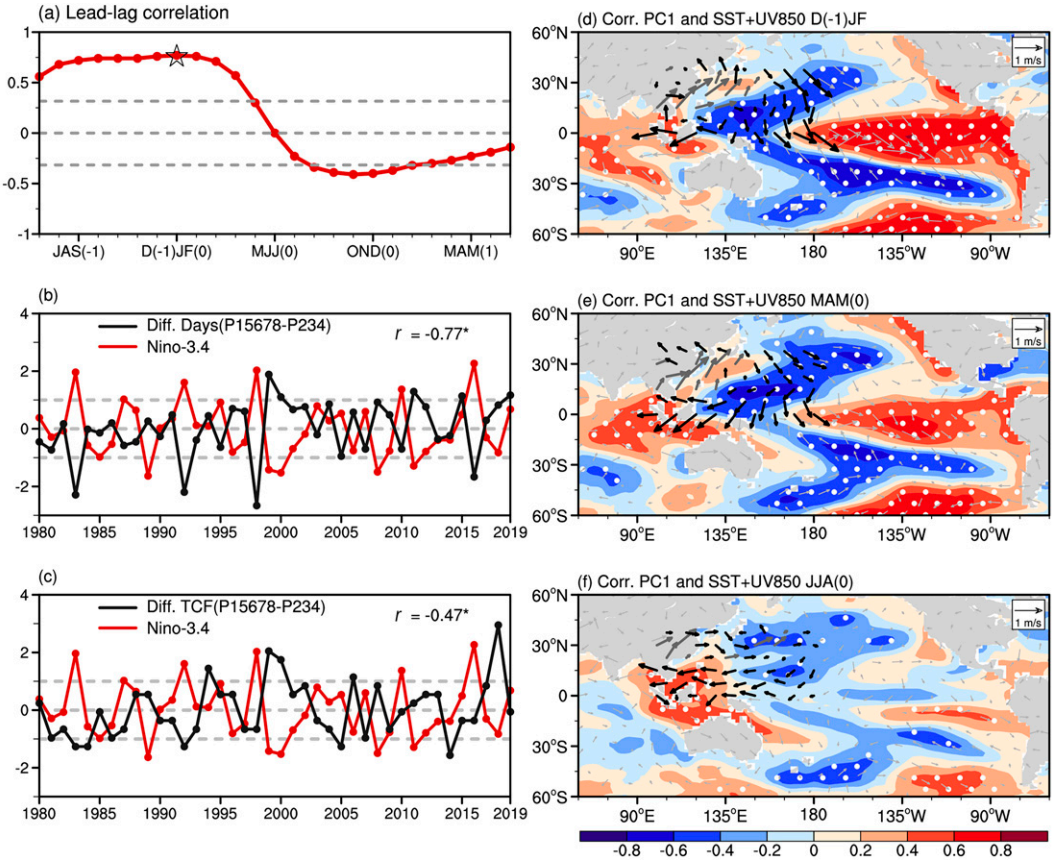

FIG. 11. (a) Lead–lag correlations between PC1 and the Niño-3.4 index. The star marks the maximum correlation. (b) Standardized time series of the difference between the frequency of occurrence for phases 1 and 5–8 and phases 2–4 occurrence and Niño-3.4. (c) Standardized time series of the TC genesis frequency difference between phases 1 and 5–8 and phases 2–4 and Niño-3.4. Correlation between PC1 for May–October and SST (shaded) and 850-hPa winds (vectors; reference vector at top right) in (d) December–February, (e) March–May, and (f) June–August. Black vectors and white dots in (d)–(f) indicate significant correlations at the 95% confidence level. An asterisk in (a)–(c) indicates that the correlation is significant at the 95% confidence level.

BSISO over the WNP basin, while there appears to be a strong impact of prior ENSO on TC genesis latitude via changes in BSISO phase occurrence frequency. The ENSO-BSISO-TC relationship warrants additional study.

Interannual BSISO activity has shown a substantial interdecadal shift since the late 1990s, consistent with a poleward shift in WNP TC genesis during recent decades. We decomposed the annual mean latitude of TC location metrics and found that the

TABLE 1. Mean latitude of TCs and the three contributing terms for the two subperiods. The term $\overline{\delta}$ means the TC genesis latitude, consisting of the climatological TC genesis latitudes weighted by their frequency for each subperiod. The term δ_P means the deviation of the relative frequency, and the term δ_{LAT} means the deviations of the annual-mean latitude from its climatological average for each subperiod. The term δ_{LATP} means the interannual covariance between δ_P and δ_{LAT}, indicating the covariability of TC genesis frequency and TC genesis latitude. Years with PC1 > 0 and PC1 < 0 were examined.

	1980–98		1999–2019	
	PC1 > 0	PC1 < 0	PC1 > 0	PC1 < 0
$\overline{\delta}$	7.7	9.5	7.7	9.5
δ_P	2.6	−2.6	−2.6	2.6
δ_{LAT}	−0.2	−0.3	0.2	0.3
δ_{LATP}	−0.1	0.1	−0.1	0.1
Total	10.0	6.7	5.2	12.5
LAT	16.7		17.7	

TABLE 2. As in Table 1, but for years with PC1 > 0.8 STD, PC1 < −0.8 STD, and all remaining neutral years.

	1980–98			1999–2019		
	PC1 > 0.8	Neutral	PC1 < −0.8	PC1 > 0.8	Neutral	PC1 < −0.8
$\overline{\delta}$	2.0	11.4	3.6	2.0	11.4	3.6
δ_P	0.5	2.2	−2.6	−0.5	−2.2	2.6
δ_{LAT}	−0.1	−0.1	−0.4	0.1	0.1	0.4
δ_{LATP}	−0.03	−0.02	0.3	−0.03	−0.02	0.3
Total	2.4	13.5	0.9	1.6	9.3	6.9
LAT		16.8			17.8	

poleward shift of WNP TC genesis during recent decades is mainly due to more strong negative PC1 years associated with increased BSISO residence time over the subtropical SCS–WNP and increased covariability of TC genesis frequency and TC genesis latitude. Since 1998, strong negative PC1 years have become more frequent, while more frequent strong positive PC1 years occurred before 1998 (Fig. 5c). Interdecadal changes in BSISO activity associated with phase frequency changes in phases 1 and 5–8 and phases 2–4 may be tied to the tropical Pacific climate shift (e.g., shifting ENSO conditions and an Indo-Pacific warm pool expansion). The associated physical mechanisms for the BSISO–tropical Pacific climate shift relationship warrant further investigation.

Acknowledgments. This research was jointly supported by the National Natural Science Foundation of China (Grants 42192551, 41922033, and 41730961) and the Six Talent Peaks project in Jiangsu Province (JY-100). P. Klotzbach would like to acknowledge a grant from the G. Unger Vetlesen Foundation. We acknowledge the High Performance Computing Center of Nanjing University of Information Science and Technology for their support of this work.

Data availability statement. The data used in this manuscript are available from the following sources: JTWC TC best track dataset: http://www.metoc.navy.mil/jtwc/jtwc.html/western-pacific; NCEP-DOE Reanalysis 2 monthly mean data: https://psl.noaa.gov/data/gridded/data.ncep.reanalysis2.html; ERSSTv5 data: https://www.ncdc.noaa.gov/data-access/marineocean-data/extended-reconstructed-sea-surface-temperature-ersst-v5; Niño-3.4 index: https://psl.noaa.gov/data/correlation/nina34.data; and OLR data: https://psl.noaa.gov/data/gridded/data.interp_OLR.html.

REFERENCES

Adames, Á. F., J. M. Wallace, and J. M. Monteiro, 2016: Seasonality of the structure and propagation characteristics of the MJO. *J. Atmos. Sci.*, **73**, 3511–3526, https://doi.org/10.1175/JAS-D-15-0232.1.

Aiyyer, A., and J. Molinari, 2008: MJO and tropical cyclogenesis in the Gulf of Mexico and eastern Pacific: Case study and idealized numerical modeling. *J. Atmos. Sci.*, **65**, 2691–2704, https://doi.org/10.1175/2007JAS2348.1.

Bessafi, M., and M. C. Wheeler, 2006: Modulation of south Indian Ocean tropical cyclones by the Madden–Julian oscillation and convectively coupled equatorial waves. *Mon. Wea. Rev.*, **134**, 638–656, https://doi.org/10.1175/MWR3087.1.

Bui, H. X., and E. D. Maloney, 2019: Mechanisms for global warming impacts on Madden–Julian oscillation precipitation amplitude. *J. Climate*, **32**, 6961–6975, https://doi.org/10.1175/JCLI-D-19-0051.1.

Cai, Y., X. Han, H. Zhao, P. J. Klotzbach, L. Wu, G. B. Raga, and C. Wang, 2022: Enhanced predictability of rapidly intensifying tropical cyclones over the western North Pacific associated with snow depth changes over the Tibetan Plateau. *J. Climate*, **35**, 2093–2110, https://doi.org/10.1175/JCLI-D-21-0758.1.

Camargo, S. J., M. C. Wheeler, and A. H. Sobel, 2009: Diagnosis of the MJO modulation of tropical cyclogenesis using an empirical index. *J. Atmos. Sci.*, **66**, 3061–3074, https://doi.org/10.1175/2009JAS3101.1.

Chen, G., and B. Wang, 2021: Diversity of the boreal summer intraseasonal oscillation. *J. Geophys. Res. Atmos.*, **126**, e2020JD034137, https://doi.org/10.1029/2020JD034137.

Chu, P.-S., 2002: Large-scale circulation features associated with decadal variations of tropical cyclone activity over the central North Pacific. *J. Climate*, **15**, 2678–2689, https://doi.org/10.1175/1520-0442(2002)015<2678:LSCFAW>2.0.CO;2.

Dasgupta, P., M. K. Roxy, R. Chattopadhyay, C. V. Naidu, and A. Metya, 2021: Interannual variability of the frequency of MJO phases and its association with two types of ENSO. *Sci. Rep.*, **11**, 11541, https://doi.org/10.1038/s41598-021-91060-2.

Emanuel, K. A., and D. S. Nolan, 2004: Tropical cyclone activity and the global climate system. *26th Conf. on Hurricanes and Tropical Meteorology*, Miami, FL, Amer. Meteor. Soc., 10A.2, https://ams.confex.com/ams/26HURR/techprogram/paper_75463.htm.

Feng, X., N. P. Klingaman, and K. I. Hodges, 2021: Poleward migration of western North Pacific tropical cyclones related to changes in cyclone seasonality. *Nat. Commun.*, **12**, 6210, https://doi.org/10.1038/s41467-021-26369-7.

Han, X., H. Zhao, X. Li, G. B. Raga, C. Wang, and Q. Li, 2020: Modulation of boreal extended summer tropical cyclogenesis over the northwest Pacific by the quasi-biweekly oscillation under different El Niño-Southern Oscillation phases. *Int. J. Climatol.*, **40**, 858–873, https://doi.org/10.1002/joc.6244.

Holland, G. J., 1995: Scale interaction in the western Pacific monsoon. *Meteor. Atmos. Phys.*, **56**, 57–79, https://doi.org/10.1007/BF01022521.

Hsu, H.-H., and C.-H. Weng, 2001: Northwestward propagation of the intraseasonal oscillation in the western North Pacific during the boreal summer: Structure and mechanism. *J. Climate*, **14**, 3834–3850, https://doi.org/10.1175/1520-0442(2001)014<3834:NPOTIO>2.0.CO;2.

——, ——, and C.-H. Wu, 2004: Contrasting characteristics between the northward and eastward propagation of the intraseasonal oscillation during the boreal summer. *J. Climate*, **17**,

727–743, https://doi.org/10.1175/1520-0442(2004)017<0727:CCBTNA>2.0.CO;2.

Hsu, P.-C., J.-Y. Lee, and K.-J. Ha, 2016: Influence of boreal summer intraseasonal oscillation on rainfall extremes in southern China. *Int. J. Climatol.*, **36**, 1403–1412, https://doi.org/10.1002/joc.4433.

Hu, C., C. Zhang, S. Yang, D. Chen, and S. He, 2018: Perspective on the northwestward shift of autumn tropical cyclogenesis locations over the western North Pacific from shifting ENSO. *Climate Dyn.*, **51**, 2455–2465, https://doi.org/10.1007/s00382-017-4022-1.

Huang, B., and Coauthors, 2017: Extended reconstructed sea surface temperature, version 5 (ERSSTv5): Upgrades, validations, and intercomparisons. *J. Climate*, **30**, 8179–8205, https://doi.org/10.1175/JCLI-D-16-0836.1.

Huang, P., C. Chou, and R. Huang, 2011: Seasonal modulation of tropical intraseasonal oscillations on tropical cyclone geneses in the western North Pacific. *J. Climate*, **24**, 6339–6352, https://doi.org/10.1175/2011JCLI4200.1.

Jiang, X., 2017: Key processes for the eastward propagation of the Madden-Julian oscillation based on multimodel simulations. *J. Geophys. Res. Atmos.*, **122**, 755–770, https://doi.org/10.1002/2016JD025955.

——, T. Li, and B. Wang, 2004: Structures and mechanisms of the northward propagating boreal summer intraseasonal oscillation. *J. Climate*, **17**, 1022–1039, https://doi.org/10.1175/1520-0442(2004)017<1022:SAMOTN>2.0.CO;2.

——, M. Zhao, and D. E. Waliser, 2012: Modulation of tropical cyclones over the eastern Pacific by the intraseasonal variability simulated in an AGCM. *J. Climate*, **25**, 6524–6538, https://doi.org/10.1175/JCLI-D-11-00531.1.

——, Á. F. Adames, M. Zhao, D. Waliser, and E. Maloney, 2018: A unified moisture mode framework for seasonality of the Madden–Julian oscillation. *J. Climate*, **31**, 4215–4224, https://doi.org/10.1175/JCLI-D-17-0671.1.

Kanamitsu, M., W. Ebisuzaki, J. Woollen, S.-K. Yang, J. J. Hnilo, M. Fiorino, and G. L. Potter, 2002: NCEP-DOE AMIP-II reanalysis (R-2). *Bull. Amer. Meteor. Soc.*, **83**, 1631–1644, https://doi.org/10.1175/BAMS-83-11-1631.

Kikuchi, K., and B. Wang, 2009: Global perspective of the quasi-biweekly oscillation. *J. Climate*, **22**, 1340–1359, https://doi.org/10.1175/2008JCLI2368.1.

——, ——, and Y. Kajikawa, 2012: Bimodal representation of the tropical intraseasonal oscillation. *Climate Dyn.*, **38**, 1989–2000, https://doi.org/10.1007/s00382-011-1159-1.

Kim, H.-M., 2017: The impact of the mean moisture bias on the key physics of MJO propagation in the ECMWF reforecast. *J. Geophys. Res. Atmos.*, **122**, 7772–7784, https://doi.org/10.1002/2017JD027005.

Kim, J.-H., C.-H. Ho, H.-S. Kim, C.-H. Sui, and S. K. Park, 2008: Systematic variation of summertime tropical cyclone activity in the western North Pacific in relation to the Madden–Julian oscillation. *J. Climate*, **21**, 1171–1191, https://doi.org/10.1175/2007JCLI1493.1.

Kossin, J. P., K. A. Emanuel, and S. J. Camargo, 2016: Past and projected changes in western North Pacific tropical cyclone exposure. *J. Climate*, **29**, 5725–5739, https://doi.org/10.1175/JCLI-D-16-0076.1.

Lau, K.-M., and P. H. Chan, 1985: Aspects of the 40–50 day oscillation during the northern winter as inferred from outgoing longwave radiation. *Mon. Wea. Rev.*, **113**, 1889–1909, https://doi.org/10.1175/1520-0493(1985)113<1889:AOTDOD>2.0.CO;2.

Lee, J.-Y., B. Wang, M. C. Wheeler, X. Fu, D. E. Waliser, and I.-S. Kang, 2013: Real-time multivariate indices for the boreal summer intraseasonal oscillation over the Asian summer monsoon region. *Climate Dyn.*, **40**, 493–509, https://doi.org/10.1007/s00382-012-1544-4.

Li, R. C. Y., and W. Zhou, 2013: Modulation of western North Pacific tropical cyclone activity by the ISO. Part I: Genesis and intensity. *J. Climate*, **26**, 2904–2918, https://doi.org/10.1175/JCLI-D-12-00210.1.

Liebmann, B., H. H. Hendon, and J. D. Glick, 1994: The relationship between tropical cyclones of the western Pacific and Indian Oceans and the Madden-Julian oscillation. *J. Meteor. Soc. Japan*, **72**, 401–412, https://doi.org/10.2151/jmsj1965.72.3_401.

Lin, A., and T. Li, 2008: Energy spectrum characteristics of boreal summer intraseasonal oscillations: Climatology and variations during the ENSO developing and decaying phases. *J. Climate*, **21**, 6304–6320, https://doi.org/10.1175/2008JCLI2331.1.

Lin, H., 2019: Long-lead ENSO control of the boreal summer intraseasonal oscillation in the East Asian-western North Pacific region. *npj Climate Atmos. Sci.*, **2**, 31, https://doi.org/10.1038/s41612-019-0088-2.

——, G. Brunet, and B. Yu, 2015: Interannual variability of the Madden-Julian oscillation and its impact on the North Atlantic Oscillation in the boreal winter. *Geophys. Res. Lett.*, **42**, 5571–5576, https://doi.org/10.1002/2015GL064547.

Liu, F., T. Li, H. Wang, L. Deng, and Y. Zhang, 2016: Modulation of boreal summer intraseasonal oscillations over the western North Pacific by ENSO. *J. Climate*, **29**, 7189–7201, https://doi.org/10.1175/JCLI-D-15-0831.1.

——, J. Zhao, X. Fu, and G. Huang, 2018: The role of shallow convection in promoting the northward propagation of boreal summer intraseasonal oscillation. *Theor. Appl. Climatol.*, **131**, 1387–1395, https://doi.org/10.1007/s00704-017-2064-2.

——, B. Wang, Y. Ouyang, H. Wang, S. Qiao, G. Chen, and W. Dong, 2022: Intraseasonal variability of global land monsoon precipitation and its recent trend. *npj Climate Atmos. Sci.*, **5**, 30, https://doi.org/10.1038/s41612-022-00253-7.

Liu, K. S., and J. C. L. Chan, 2013: Inactive period of western North Pacific tropical cyclone activity in 1998–2011. *J. Climate*, **26**, 2614–2630, https://doi.org/10.1175/JCLI-D-12-00053.1.

Madden, R. A., and P. R. Julian, 1971: Detection of a 40–50 day oscillation in the zonal wind in the tropical Pacific. *J. Atmos. Sci.*, **28**, 702–708, https://doi.org/10.1175/1520-0469(1971)028<0702:DOADOI>2.0.CO;2.

Maloney, E. D., and D. L. Hartmann, 2000a: Modulation of hurricane activity in the Gulf of Mexico by the Madden–Julian oscillation. *Science*, **287**, 2002–2004, https://doi.org/10.1126/science.287.5460.2002.

——, and ——, 2000b: Modulation of eastern North Pacific hurricanes by the Madden–Julian oscillation. *J. Climate*, **13**, 1451–1460, https://doi.org/10.1175/1520-0442(2000)013<1451:MOENPH>2.0.CO;2.

——, and M. J. Dickinson, 2003: The intraseasonal oscillation and the energetics of summertime tropical western North Pacific synoptic-scale disturbances. *J. Atmos. Sci.*, **60**, 2153–2168, https://doi.org/10.1175/1520-0469(2003)060<2153:TIOATE>2.0.CO;2.

——, Á. F. Adames, and H. X. Bui, 2019: Madden–Julian oscillation changes under anthropogenic warming. *Nat. Climate Change*, **9**, 26–33, https://doi.org/10.1038/s41558-018-0331-6.

Moon, I.-J., S.-H. Kim, P. Klotzbach, and J. C. L. Chan, 2015: Roles of interbasin frequency changes in the poleward shifts

of the maximum intensity location of tropical cyclones. *Environ. Res. Lett.*, **10**, 104004, https://doi.org/10.1088/1748-9326/10/10/104004.

Moon, J.-Y., B. Wang, S.-S. Lee, and K.-J. Ha, 2018: An intraseasonal genesis potential index for tropical cyclones during Northern Hemisphere summer. *J. Climate*, **31**, 9055–9071, https://doi.org/10.1175/JCLI-D-18-0515.1.

Nakano, M., F. Vitart, and K. Kikuchi, 2021: Impact of the boreal summer intraseasonal oscillation on typhoon tracks in the western North Pacific and the prediction skill of the ECMWF model. *Geophys. Res. Lett.*, **48**, e2020GL091505, https://doi.org/10.1029/2020GL091505.

Nakazawa, T., 1986: Intraseasonal variations of OLR in the tropics during the FGGE year. *J. Meteor. Soc. Japan*, **64**, 17–34, https://doi.org/10.2151/jmsj1965.64.1_17.

——, 1988: Tropical super clusters within intraseasonal variations over the western Pacific. *J. Meteor. Soc. Japan*, **66**, 823–839, https://doi.org/10.2151/jmsj1965.66.6_823.

North, G. R., T. L. Bell, R. F. Cahalan, and F. J. Moeng, 1982: Sampling errors in the estimation of empirical orthogonal functions. *Mon. Wea. Rev.*, **110**, 699–706, https://doi.org/10.1175/1520-0493(1982)110<0699:SEITEO>2.0.CO;2.

Pohl, B., and A. J. Matthews, 2007: Observed changes in the lifetime and amplitude of the Madden–Julian oscillation associated with interannual ENSO sea surface temperature anomalies. *J. Climate*, **20**, 2659–2674, https://doi.org/10.1175/JCLI4230.1.

Qin, N., L. Wu, Q. Liu, and X. Zhou, 2023: Driving forces of extreme updrafts associated with convective bursts in the eyewall of a simulated tropical cyclone. *J. Geophys. Res. Atmos.*, **128**, e2022JD037061, https://doi.org/10.1029/2022JD037061.

Ren, P., H.-L. Ren, J.-X. Fu, J. Wu, and L. Du, 2018: Impact of boreal summer intraseasonal oscillation on rainfall extremes in southeastern China and its predictability in CFSv2. *J. Geophys. Res. Atmos.*, **123**, 4423–4442, https://doi.org/10.1029/2017JD028043.

Roxy, M. K., P. Dasgupta, M. J. McPhaden, T. Suematsu, C. Zhang, and D. Kim, 2019: Twofold expansion of the Indo-Pacific warm pool warps the MJO life cycle. *Nature*, **575**, 647–651, https://doi.org/10.1038/s41586-019-1764-4.

Sobel, A. H., and C. S. Bretherton, 1999: Development of synoptic-scale disturbances over the summertime tropical northwest Pacific. *J. Atmos. Sci.*, **56**, 3106–3127, https://doi.org/10.1175/1520-0469(1999)056<3106:DOSSDO>2.0.CO;2.

——, and E. D. Maloney, 2000: Effect of ENSO and the MJO on western North Pacific tropical cyclones. *Geophys. Res. Lett.*, **27**, 1739–1742, https://doi.org/10.1029/1999GL011043.

——, and E. Maloney, 2013: Moisture modes and the eastward propagation of the MJO. *J. Atmos. Sci.*, **70**, 187–192, https://doi.org/10.1175/JAS-D-12-0189.1.

Song, J., and P. J. Klotzbach, 2018: What has controlled the poleward migration of annual averaged location of tropical cyclone lifetime maximum intensity over the western North Pacific since 1961? *Geophys. Res. Lett.*, **45**, 1148–1156, https://doi.org/10.1002/2017GL076883.

Suematsu, T., and H. Miura, 2018: Zonal SST difference as a potential environmental factor supporting the longevity of the Madden–Julian oscillation. *J. Climate*, **31**, 7549–7564, https://doi.org/10.1175/JCLI-D-17-0822.1.

——, ——, C. Kodama, and D. Takasuka, 2022: Deceleration of Madden–Julian oscillation speed in NICAM AMIP-type simulation associated with biases in the Walker circulation strength. *Geophys. Res. Lett.*, **49**, e2022GL098628, https://doi.org/10.1029/2022GL098628.

Takaya, Y., Y. Kosaka, M. Watanabe, and S. Maeda, 2021: Skilful predictions of the Asian summer monsoon one year ahead. *Nat. Commun.*, **12**, 2094, https://doi.org/10.1038/s41467-021-22299-6.

Tao, L., J. Zhao, and T. Li, 2015: Trend analysis of tropical intraseasonal oscillations in the summer and winter during 1982–2009. *Int. J. Climatol.*, **35**, 3969–3978, https://doi.org/10.1002/joc.4258.

Teng, H., and B. Wang, 2003: Interannual variations of the boreal summer intraseasonal oscillation in the Asian–Pacific region. *J. Climate*, **16**, 3572–3584, https://doi.org/10.1175/1520-0442(2003)016<3572:IVOTBS>2.0.CO;2.

Wang, B., and H. Rui, 1990: Synoptic climatology of transient tropical intraseasonal convection anomalies: 1975–1985. *Meteor. Atmos. Phys.*, **44**, 43–61, https://doi.org/10.1007/BF01026810.

——, and X. Xie, 1997: A model for the boreal summer intraseasonal oscillation. *J. Atmos. Sci.*, **54**, 72–86, https://doi.org/10.1175/1520-0469(1997)054<0072:AMFTBS>2.0.CO;2.

——, and J.-Y. Moon, 2017: An anomalous genesis potential index for MJO modulation of tropical cyclones. *J. Climate*, **30**, 4021–4035, https://doi.org/10.1175/JCLI-D-16-0749.1.

——, R. Wu, and X. Fu, 2000: Pacific–East Asian teleconnection: How does ENSO affect East Asian climate? *J. Climate*, **13**, 1517–1536, https://doi.org/10.1175/1520-0442(2000)013<1517:PEATHD>2.0.CO;2.

——, G. Chen, and F. Liu, 2019: Diversity of the Madden-Julian oscillation. *Sci. Adv.*, **5**, eaax0220, https://doi.org/10.1126/sciadv.aax0220.

Wang, S., and A. H. Sobel, 2022: A unified moisture mode theory for the Madden–Julian oscillation and the boreal summer intraseasonal oscillation. *J. Climate*, **35**, 1267–1291, https://doi.org/10.1175/JCLI-D-21-0361.1.

Wheeler, M., and K. M. Weickmann, 2001: Real-time monitoring and prediction of modes of coherent synoptic to intraseasonal tropical variability. *Mon. Wea. Rev.*, **129**, 2677–2694, https://doi.org/10.1175/1520-0493(2001)129<2677:RTMAPO>2.0.CO;2.

——, and H. H. Hendon, 2004: An all-season real-time multivariate MJO index: Development of an index for monitoring and prediction. *Mon. Wea. Rev.*, **132**, 1917–1932, https://doi.org/10.1175/1520-0493(2004)132<1917:AARMMI>2.0.CO;2.

Wolding, B. O., E. D. Maloney, S. Henderson, and M. Branson, 2017: Climate change and the Madden-Julian oscillation: A vertically resolved weak temperature gradient analysis. *J. Adv. Model. Earth Syst.*, **9**, 307–331, https://doi.org/10.1002/2016MS000843.

Wu, N., Y. Li, J. Li, L.-C. Feng, and F. Liu, 2021: Decadal changes of the intraseasonal oscillation during 1979–2016. *Adv. Climate Change Res.*, **12**, 772–782, https://doi.org/10.1016/j.accre.2021.10.001.

Xie, S.-P., K. Hu, J. Hafner, H. Tokinaga, Y. Du, G. Huang, and T. Sampe, 2009: Indian Ocean capacitor effect on Indo–western Pacific climate during the summer following El Niño. *J. Climate*, **22**, 730–747, https://doi.org/10.1175/2008JCLI2544.1.

——, Y. Kosaka, Y. Du, K. Hu, J. S. Chowdary, and G. Huang, 2016: Indo-western Pacific Ocean capacitor and coherent climate anomalies in post-ENSO summer: A review. *Adv. Atmos. Sci.*, **33**, 411–432, https://doi.org/10.1007/s00376-015-5192-6.

Yamaura, T., and Y. Kajikawa, 2017: Decadal change in the boreal summer intraseasonal oscillation. *Climate Dyn.*, **48**, 3003–3014, https://doi.org/10.1007/s00382-016-3247-8.

Yasunari, T., 1979: Cloudiness fluctuations associated with the Northern Hemisphere summer monsoon. *J. Meteor. Soc. Japan*, **57**, 227–242, https://doi.org/10.2151/jmsj1965.57.3_227.

——, 1981: Structure of an Indian summer monsoon system with around 40-day period. *J. Meteor. Soc. Japan*, **59**, 336–354, https://doi.org/10.2151/jmsj1965.59.3_336.

Yun, K.-S., K.-H. Seo, and K.-J. Ha, 2010: Interdecadal change in the relationship between ENSO and the intraseasonal oscillation in East Asia. *J. Climate*, **23**, 3599–3612, https://doi.org/10.1175/2010JCLI3431.1.

Zhang, C., 2013: Madden–Julian oscillation: Bridging weather and climate. *Bull. Amer. Meteor. Soc.*, **94**, 1849–1870, https://doi.org/10.1175/BAMS-D-12-00026.1.

——, and M. Dong, 2004: Seasonality in the Madden–Julian oscillation. *J. Climate*, **17**, 3169–3180, https://doi.org/10.1175/1520-0442(2004)017<3169:SITMO>2.0.CO;2.

Zhao, C., and T. Li, 2019: Basin dependence of the MJO modulating tropical cyclone genesis. *Climate Dyn.*, **52**, 6081–6096, https://doi.org/10.1007/s00382-018-4502-y.

Zhao, H., X. Jiang, and L. Wu, 2015a: Modulation of northwest Pacific tropical cyclone genesis by the intraseasonal variability. *J. Meteor. Soc. Japan*, **93**, 81–97, https://doi.org/10.2151/jmsj.2015-006.

——, R. Yoshida, and G. B. Raga, 2015b: Impact of the Madden–Julian oscillation on western North Pacific tropical cyclogenesis associated with large-scale patterns. *J. Appl. Meteor. Climatol.*, **54**, 1413–1429, https://doi.org/10.1175/JAMC-D-14-0254.1.

——, S. Chen, P. J. Klotzbach, and G. B. Raga, 2018: Impact of the extended boreal summer intraseasonal oscillation on western North Pacific tropical cloud cluster genesis productivity. *J. Climate*, **31**, 9175–9191, https://doi.org/10.1175/JCLI-D-18-0113.1.

——, X. Jiang, L. Wu, and P. J. Klotzbach, 2019a: Multi-scale interactions of equatorial waves associated with tropical cyclogenesis over the western North Pacific. *Climate Dyn.*, **52**, 3023–3038, https://doi.org/10.1007/s00382-018-4307-z.

——, J. Zhang, P. J. Klotzbach, and S. Chen, 2019b: Recent increased covariability of tropical cyclogenesis latitude and longitude over the western North Pacific during the extended boreal summer. *J. Climate*, **32**, 8167–8179, https://doi.org/10.1175/JCLI-D-19-0009.1.

——, Y. Lu, X. Jiang, P. J. Klotzbach, L. Wu, and J. Cao, 2022: A statistical intraseasonal prediction model of extended boreal summer western North Pacific tropical cyclone genesis. *J. Climate*, **35**, 2459–2478, https://doi.org/10.1175/JCLI-D-21-0110.1.

Zhou, W., D. Yang, S.-P. Xie, and J. Ma, 2020: Amplified Madden–Julian oscillation impacts in the Pacific–North America region. *Nat. Climate Change*, **10**, 654–660, https://doi.org/10.1038/s41558-020-0814-0.